Journal of the European Ceramic Society 44 (2024) 729–737

Contents lists available at ScienceDirect

Journal of the European Ceramic Society

journal homepage: www.elsevier.com/locate/jeurceramsoc

From outer space to inside the body: Ultra-high temperature ceramic matrix composites for biomedical applications

Luca Zoli [a], Francesca Servadei [a,*], Giada Bassi [a,b], Arianna Rossi [a,c], Monica Montesi [a], Antonio Vinci [a], Diletta Sciti [a], Silvia Panseri [a]

[a] CNR-ISSMC (former ISTEC), National Research Council of Italy - Institute of Science, Technology and Sustainability for Ceramics, Via Granarolo 64, 48018 Faenza, RA, Italy
[b] Department of Neuroscience, Imaging and Clinical Sciences, University of Studies "G. D'Annunzio", 66100 Chieti, CH, Italy
[c] Department of Chemical, Biological, Pharmaceutical and Environmental Sciences, University of Studies of Messina, 98122 Messina, ME, Italy

ARTICLE INFO

Keywords:
Ceramic matrix composite
Cytocompatibility
Zirconium diboride
Pitch-based carbon fibers
Biomedical ceramics

ABSTRACT

Ultra-high temperature ceramic matrix composites (UHTCMCs) are a new class of carbon fiber-reinforced non-brittle ceramics possessing a unique combination of properties (e.g. high fracture toughness, damage tolerance and corrosion resistance), originally developed for use in extreme hot and harsh environments, such as those found in aerospace and industrial applications. Interconnections between very remote fields more and more frequently come across to discover new solutions. In this study, we investigated the compression strength and cytotoxicity of UHTCMCs designed as biomaterials for future applications inside the body. Indeed, despite the advancements in the designing, manufacturing and surface modification, current prostheses are made of metals or alloys with well-known disadvantages. Near-fully dense C_f/ZrB_2-SiC composites were manufactured through slurry impregnation followed by spark plasma sintering. A preliminary biological in vitro study demonstrated materials' lack of cytotoxicity, making them promising candidates for further investigation for biomedical purposes.

1. Introduction

In the last century, there are several examples of materials developed for one specific purpose that have turned out to be suitable for other completely different applications. Two advanced ceramics, silicon nitride (Si_3N_4) and silicon carbide (SiC), were widely investigated for several structural and functional high-temperature applications under harsh and wear environments. Gas turbines, heat shields, ballistic protections, semiconductors are only some components realized with these materials. Their use in medical applications has been a surprise. While keeping all their engineering properties of wear resistance and high strength, their unique chemical properties have only recently shown a role in biological processes. For example, the healing of soft and hard tissues, and the inhibition of bacterial and/or viral proliferation were observed after immersion of Si_3N_4 specimens in an aqueous environment [1,2]. These beneficial effects seem to be caused by the slow evolution of silicon and nitrogen from Si_3N_4 surface, making that environment toxic to bacteria and nourishing to eukaryotic cells. Similarly, SiC has shown its bio- and hemo- compatibility when used as heart stent coatings, diagnostic neural implants and sensors for human healthcare (e.g. glucose and hemoglobin detection) [3].

However, one of the main issues for a wide range of applications of advanced ceramics is the intrinsic brittleness [4] that drastically limits their use in the fabrication of medical devices for hard tissues, such as dental and orthopedic prostheses that require specific mechanical performance. In detail, the part of the prosthesis that is fixed within the bone/jaw (e.g. stem for hip prosthesis, dental screw) is usually made of metals or alloys due to their overall high strength and damage tolerance [5]. These include titanium, tantalum and alloys of aluminum, vanadium, cobalt, chromium and molybdenum, that show high mechanical strength and excellent toughness, essential for load bearing applications, durability and resistance to wear, good ductility, but they do not show any bioactivity. In addition, the main disadvantage is that metal can be corroded due to chemical reaction with the body enzymes and acids causing metal ion toxicity in the body. For this reason, several polymeric and/or ceramic coatings have been explored in the last decades to make the metallic prostheses more biocompatible and bioactive [6,7].

Other attempts proposed the use of polymers [8] as raw materials to

* Corresponding author.
E-mail address: francesca.servadei@issmc.cnr.it (F. Servadei).

https://doi.org/10.1016/j.jeurceramsoc.2023.10.007
Received 27 June 2023; Received in revised form 2 October 2023; Accepted 4 October 2023
Available online 5 October 2023

design the entire medical device. Particular attention is given to the polymer polyether ether ketone (PEEK) for its anticorrosive properties, low weight, mechanical performance and the lack of a negative impact on the body environment. However, PEEK has a relatively hydrophobic surface, which limits cell adhesion. The biological inertia of PEEK makes the bone integration between the PEEK implant and the host bone tissue poor, and clinically often encounters many complications, such as implant displacement, that have led to unsatisfactory results [9].

Recent developments in the field of fiber-reinforced ultra-high temperature ceramic matrix composites (UHTCMCs) have shown how it would be possible to exploit the advantages of refractory ceramics, such as excellent thermal stability, chemical inertness, high mechanical strength, and wear resistance, while retaining the damage tolerance provided by the fiber reinforcement. Even though these materials are primarily designed for aerospace and industrial sectors characterized by extremely hot and harsh environments, where the material must withstand sudden changes in temperature above 1800 °C, their features have been widely investigated and their excellent mechanical properties are compatible with biomedical applications, such as in artificial knee replacement and cardiac stent [10–13].

In this work, for the first time to the best of our knowledge, the use of sintered UHTCMCs is proposed as an unconventional approach for biomedical purposes. A carbon fiber-reinforced ZrB_2-SiC composite was designed and manufactured by slurry impregnation and sintering (SIS) and tested to evaluate its cytocompatibility. Since it should be devoted to applications within human body, the main mechanical properties at room temperature were explored, focusing on compression strength both in axial and radial direction.

This study providing microstructural and mechanical information and a preliminary biological in vitro screening aims to investigate the potential of this novel type of composites for biomedical applications, making the first move to pave the way toward further preclinical studies to get this class of materials into service.

2. Material and methods

2.1. Materials

Commercially available powders were used for the preparation of ceramic composite materials: ZrB_2 (H.C. Starck, Grade B, Germany; specific surface area 1.0 m^2/g, particle size range 0.5–6 μm, impurities (wt%): 0.25 C, 2 O, 0.25 N, 0.1 Fe, 0.2 Hf), α-SiC (H.C. Starck, Grade UF-25, Germany; specific surface area 23–26 m^2/g, D_{50} 0.45 μm). Custom-made unidirectional high modulus carbon fiber fabrics (G. Angeloni, Italy; TCU 312) were used as carbon preforms.

2.2. Preparation of UHTCMC samples

Aqueous ZrB_2–10 vol% SiC powder mixture slurries were prepared by ball milling according to previous studies [10] adding a dispersant to prevent sedimentation of powders.

Two unidirectional carbon preforms with size 180 mm × 180 mm were impregnated with the aqueous suspension, stacked with 0/0° or 0/90° configurations by hand lay-up and cut into 9 (bilayer) discs with diameter 60 mm to obtain a multilayer block with unidirectional or balanced reinforcement.

Then, dried pellets with size 60 mm × 3 mm (Ø × height) were sintered by spark plasma sintering (SPS furnace H-HP D 25, FCT Systeme GmbH, Germany, available at ISSMC) with the goal of achieving near-full densification on the basis of previous studies [14,15]. The temperature was monitored with an optical pyrometer focused on the bottom of the upper graphite punch, about 5 mm away from the sample. The final pressure was applied at the beginning of the cycle and released at the beginning of the cooling stage.

Samples with balanced and unbalanced reinforcements were labelled as BAR and UBR samples, respectively.

2.3. Microstructural analysis

Both UBR and BAR samples were analyzed. After sintering, the bulk density was determined via weight-to-geometric volume ratio (balance accuracy ± 0.01 mg). The relative density, ρ, was calculated as the ratio of experimental to theoretical value, that was deduced using the rule of mixtures based on the starting compositions, and residual porosity was calculated as 1-ρ.

Machined surfaces and polished cross-sections were analyzed by scanning electron microscope (FE-SEM, ZEISS Sigma, Carl Zeiss Microscopy GmbH, Germany) and energy dispersive microanalysis (EDS, INCA Energy 300, Oxford Instruments, UK). The polished cross-sections were prepared by cross-cutting samples, mounting sections in epoxy resin and polishing them down to a 0.25 μm finish using a semi-automatic polishing machine (Tegramin-25, Struers, Italy), finally washed with solvents in an ultrasonic bath and cleaned with a plasma cleaner (Colibrì Plasma RF 50 KHz, Gambetti, Italy). To determine the final composition, the fiber volumetric content was determined by image analysis on SEM pictures of polished sections with a commercial software package (Image-Pro Plus® Analyzer 7.0, Media Cybernetics, U. S.A.).

The surface texture characterization of specimens for biological tests was performed before the cell-based studies using a non-contact optical profilometer (Contour GT-K 3D, Bruker, Germany). At the center of the discs, an area the size 5 mm × 5 mm was scanned along two orthogonal directions and the collected surface data were processed with the commercial software Vision64 Map.

2.4. Mechanical properties

Compressive strength (σ_c) was measured on specimens 8.0 mm × 4.0 mm × 4.0 mm (length by width by thickness) and 4.0 mm × 4.0 mm × 8.0 mm (length by width by thickness) at room temperature using a universal Zwick-Roell testing machine (mod. Z050, Germany) with crosshead speed 1 mm/min. Three bars for each type of specimen were carried out. Both UBR and BAR samples were tested in both longitudinal and transverse directions.

2.5. In vitro biological study

The selected sintered UBR and BAR discs were machined to obtain twenty smaller discs (6 mm × 1 mm, radius × thickness) for biological tests. Mouse fibroblast BALB/3T3 cell line (Clone A31, ATCC® CCL-163™) was cultured in DMEM high glucose medium (Gibco) supplemented with 10 % Calf Bovine Serum (Gibco) and 1 % Penicillin and Streptomycin solution (100 U/ml-100 μg/ml, Gibco) and kept at 37 °C under 5 % CO_2 atmosphere conditions and controlled humidity. Cells were detached from the culture flask by trypsinization and centrifuged; the cell number and viability were assessed by Trypan Blue dye exclusion test. For the biological study, each was sterilized with 70 % ethanol followed by 30 min UV irradiation under the biological laminar-flow sterile hood, and pre-soaked in cell culture medium for 1-hour incubation at 37 °C. Then the samples were seeded by carefully dropping 20 μl of cell suspension (3.0×10^4 cells) onto the upper surface, and allowing cell attachment for 30 min in the incubator, before the addition of 1 ml of cell culture medium. The cell culture medium was changed every 3 days for a total of 7 days of culture at 37 °C with 5 % CO_2 atmosphere and controlled humidity conditions. All cell-handling procedures were performed under biological laminar-flow hood and sterile conditions.

2.5.1. Cell viability evaluation

The quantitative evaluation of cell viability and proliferation was carried out by Presto Blue™ Cell Viability Reagent (Invitrogen) at day 1, 3 and 7 of culture according to manufacturer's instructions. In brief, at each time point, the samples were incubated with 10 % (v/v) Presto Blue Reagent in culture medium for two hours at 37 °C, 5 % CO_2 atmosphere

and controlled humidity conditions. Then, 200 μl were transferred in triplicate to a 96 well-plate and analyzed using the Fluoroskan™ Microplate Fluorometer (Thermo Fisher Scientific) setting the excitation wavelength equal to 544 nm, whereas the emission wavelength to 590 nm. A biological triplicate was performed for each time point.

2.5.2. Evaluation of cell morphology and cell-material interaction

Qualitative analysis of cell morphology was assessed by Actin and DAPI staining as fluorescent detection of cell actin filaments and cell nuclei at day 1, 3 and 7 of culture. Briefly, the seeded samples were fixed in 4 % (w/v) paraformaldehyde (PFA, Merck KGaA) for 15 min, followed by membranes permeabilization in PBS 1X with 0.1 % (v/v) Triton X-100 for 5 min at room temperature. Actin filaments were stained with FITC-conjugated fluorescein-phalloidin (38 nM, Invitrogen [16]) for 20 min incubation and cell nuclei were marked with nuclear stain 4'−6-Diamidino-2-phenylindole (DAPI) (Invitrogen) 300 nM in PBS 1X for 5 min. The images were acquired by the Inverted Ti-E fluorescent microscope (Nikon). For each time point, one sample was analyzed.

A further qualitative cell morphology analysis was performed by Scanning Electron Microscopy (SEM) (ESEM Quanta 200, FEI) at day 1 and 3 of culture. Briefly, the samples were washed in 0.1 M Sodium Cacodylate Buffer (pH 7.4) and fixed in 2.5 % Glutaraldehyde (Merck KGaA) solution in 0.1 M Sodium Cacodylate Buffer for 2 h at 4 °C. Then, they were washed with cacodylate buffer 0.1 M (pH 7.4) for 5 min, dehydrated using an alcohol scale and then placed in Hexamethyldisilazane reagent (HMDS, Merck KGaA) for 10 min before drying under the hood overnight. For the analysis, the samples were sputter-coated with 2 nm of Platinum-Palladium (Pt-Pd, 80:20 ratio) film and the images were acquired under high vacuum conditions. For each time point, one sample was analyzed.

2.5.3. Statistical analysis

The data of Presto Blue™ Cell Viability Reagent were reported by mean of RFU values ± standard error of the mean and they were analyzed by One-way analysis of variance (One-way ANOVA) together with Tukey's Multiple Comparisons test using GraphPad Prism Software (Version 8.0). Statistically significant differences of cell proliferation over time are reported in the graph: *p value $\leq$ 0.05 and **p value $\leq$ 0.01.

3. Results

3.1. Advantages of slurry impregnation and sintering vs SoA

The proposed process to realize the C/ZrB_2-SiC material by slurry impregnation of carbon fiber cloths and subsequent consolidation via spark plasma sintering (SPS), see Fig. 1, has several advantages compared to the State of Art (SoA) processes.

The average process time, including the preparation of slurries, impregnation of the composite and SPS cycle, is about 10 working hours. In comparison, current industrial manufacturing processes for carbon-carbon (C/C) or silicon carbide-silicon carbide (SiC/SiC) materials may even require weeks to completely densify a material [17]. The time and energy saving makes this process industrially more appealing; moreover, the water-based slurry impregnation is solvent-free and resin-free, without any formation of toxic pyrolysis byproducts (i.e. char, tar or other caustic substances deriving from heat treatments). Finally, the final composite does not require further post-treating or deposition of wear-resistant biomimetic or bioactive coatings, as the ZrB_2 and SiC grains are already embedded in the carbon fiber preform surrounding each single carbon fiber.

3.2. Microstructure of the as-sintered material

As example, the typical microstructure (cross-section) of as-prepared C/ZrB_2-SiC composites (BAR and UBR samples) is shown in Fig. 2.

The low magnification micrographs (Fig. 2a,b) evidence the layered structure in a 0/90° and 0/0 ° configurations with homogeneously distributed carbon fibers in a nearly fully dense ZrB_2/SiC matrix with no delamination. The volumetric fiber content amounted to about 50 vol% as ascertained by image analysis, while the matrix consisted of about 45 vol% ZrB_2 and 5 vol% SiC (Fig. 2c). Interlocking among fibers, SiC and ZrB_2 particles is well highlighted in Fig. 2d,e. During the sintering treatment, the high chemical compatibility of ZrB_2 with carbon led to enhanced reactivity between fiber and matrix, resulting in strong interfaces. The proposed thermal treatment at temperature close to 2000 °C and pressure of tens of MPa for few minutes time followed by a rapid cooling guaranteed a strong fiber/matrix interface without causing critical fiber damage.

As can be seen in high magnification micrograph in Fig. 2f, the presence of SiC particles (dark grey regions) at grain boundaries inhibited the excessive grain growth of bright contrast ZrB_2 (small variations in color are due to the different grain orientations) [18,19]. As a result, the microstructure was very fine-grained, with a mean ZrB_2 grain size of 2.2 μm. Similar microstructure was found for UD sample.

Surface micrographs of a specimen selected for biological analysis (Fig. 3) show a regular distribution of longitudinal fiber sections, at different magnification, interspaced with matrix grains, highlighting a low content of open porosity in the matrix. The surface finish appeared quite coarse, with Ra values of 2 μm obtained from roughness measurements. Moreover, fibers were visibly damaged. As previously mentioned [10], the matrix/fiber interface was very strong, therefore the fibers were rather worn than completely removed. Fig. 3 also shows a color-coded contour map of approximately twenty-five square

Fig. 1. Sketch of the water-based slurry impregnation and sintering process for manufacturing of UHTCMCs.

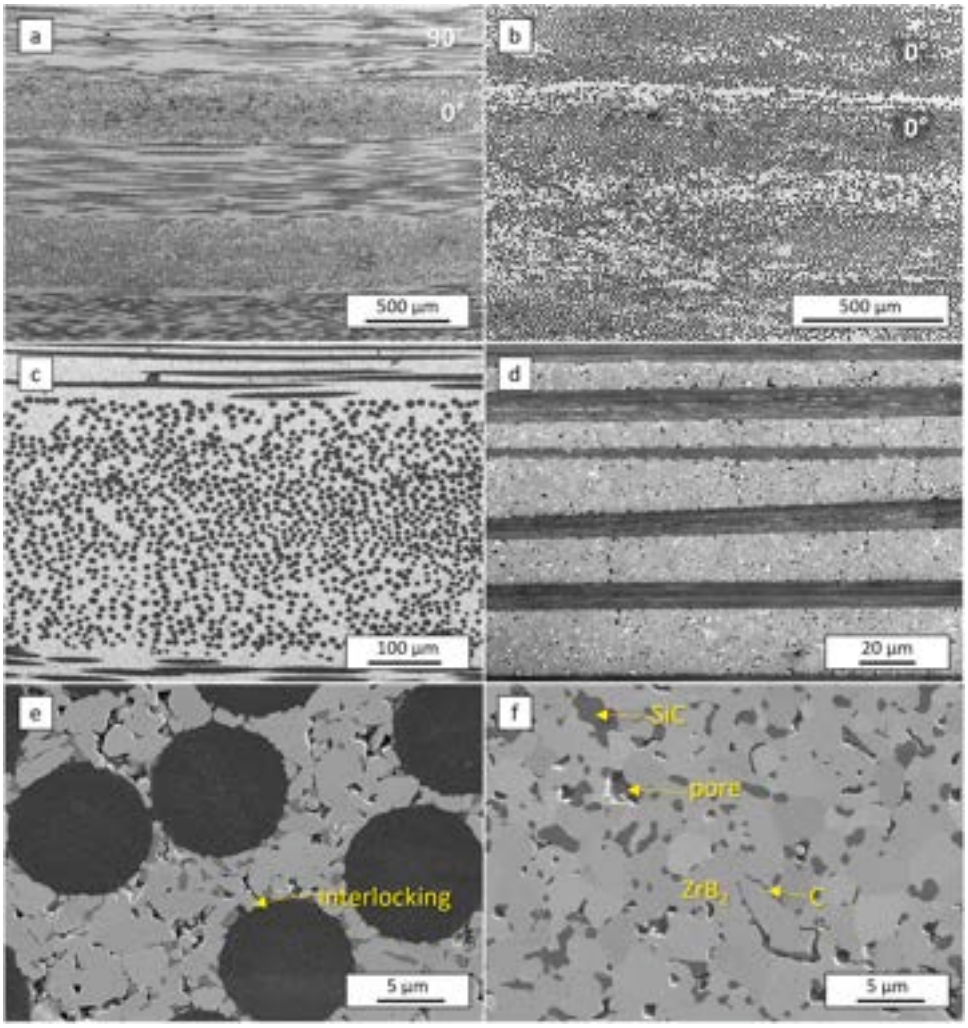

Fig. 2. Microstructure of as-sintered BAR and UBR samples: (a,b) general overview at low magnification, where black lines and dots are carbon fibers in 90° and 0° configuration, respectively, while bright contrast phase is UHTC matrix; (c) higher magnification micrograph with focus on a single layer (0°); (d,e) detail of few fibers surrounded by the matrix in 0° and 90° orientation; (f) detail of matrix.

millimeters of sample surface obtained by 3D Optical Profilometer. This analysis provided information on the depth and directionality of surface damage caused by grinding. The direction of the grooves, on the other hand, is longitudinal to the fibers.

3.3. Biological characterization

A preliminary study was performed to verify the cytocompatibility of C/ZrB_2-SiC. Murine fibroblasts, validated and widely used cell culture model for initial biological screening, were seeded on top of the samples and their viability and proliferation were evaluated up to 7 days of culture. The results in Fig. 4 show a significant increase in cell proliferation (i.e. increase of RFU) from day 1 up to day 7 (** p value $\leq$ 0.01), and from day 3 and day 7 (* p value $\leq$ 0.05) proving that there is no cytotoxicity caused by the material. These data were supported by morphological and cell-material interaction analysis through fluorescence and SEM imaging. Specifically, cell adhesion to the biomaterial affects the consequent cell proliferation and involves complex processes, especially the reorganization of cytoskeleton proteins like actin. Considering the potential application of these materials within the human body, we investigated the influence of the C/ZrB_2-SiC surface on the organization of F-actin filaments of fibroblasts. In detail, cell nuclei were visualized by Dapi and the cytoskeleton through actin filaments stained with FITC-conjugated fluorescein-phalloidin. The day after the cell seeding, the typical fibroblast phenotype well-adherent to the sample's surface was detected, suggesting a good cell adhesion (Fig. 5a–c). In addition, also the typical round shape nuclear morphology confirmed the absence of any evident cytotoxic effect (e.g. condensed chromatin and apoptotic bodies) (Fig. 5). Furthermore, it is possible to observe that over the time the cells covered all the material surface, reaching the 100 % of confluence after 7 days, (Fig. 5) without any morphological cell damage/change. These results correlate with cell viability and proliferation data detected by PrestoBlue assay after the same timeframe (Fig. 4). (These results were confirmed by the SEM images that displayed the increase in cell density over time (Fig. 5c, f, i).

3.4. Mechanical properties

Regarding the mechanical properties of these composites, both the dense ceramic matrix and the fibers provided structural properties. These composites were previously found to have high flexural (220 $\pm$ 42 MPa [10]) and tensile strengths (120 $\pm$ 7 MPa [10]), and damage tolerance (6.9 MPa·$m^{1/2}$ in [20]), while compressive strengths in longitudinal and transverse direction were reported here for the first time, see Table 1.

Similar to CMCs, the compressive strength in longitudinal direction of these UHTCMCs (i.e. 400 $\pm$ 20 MPa, see Table 1) was higher than its tensile strength (i.e. 120 $\pm$ 7 MPa for sample with 0/90° reinforcement

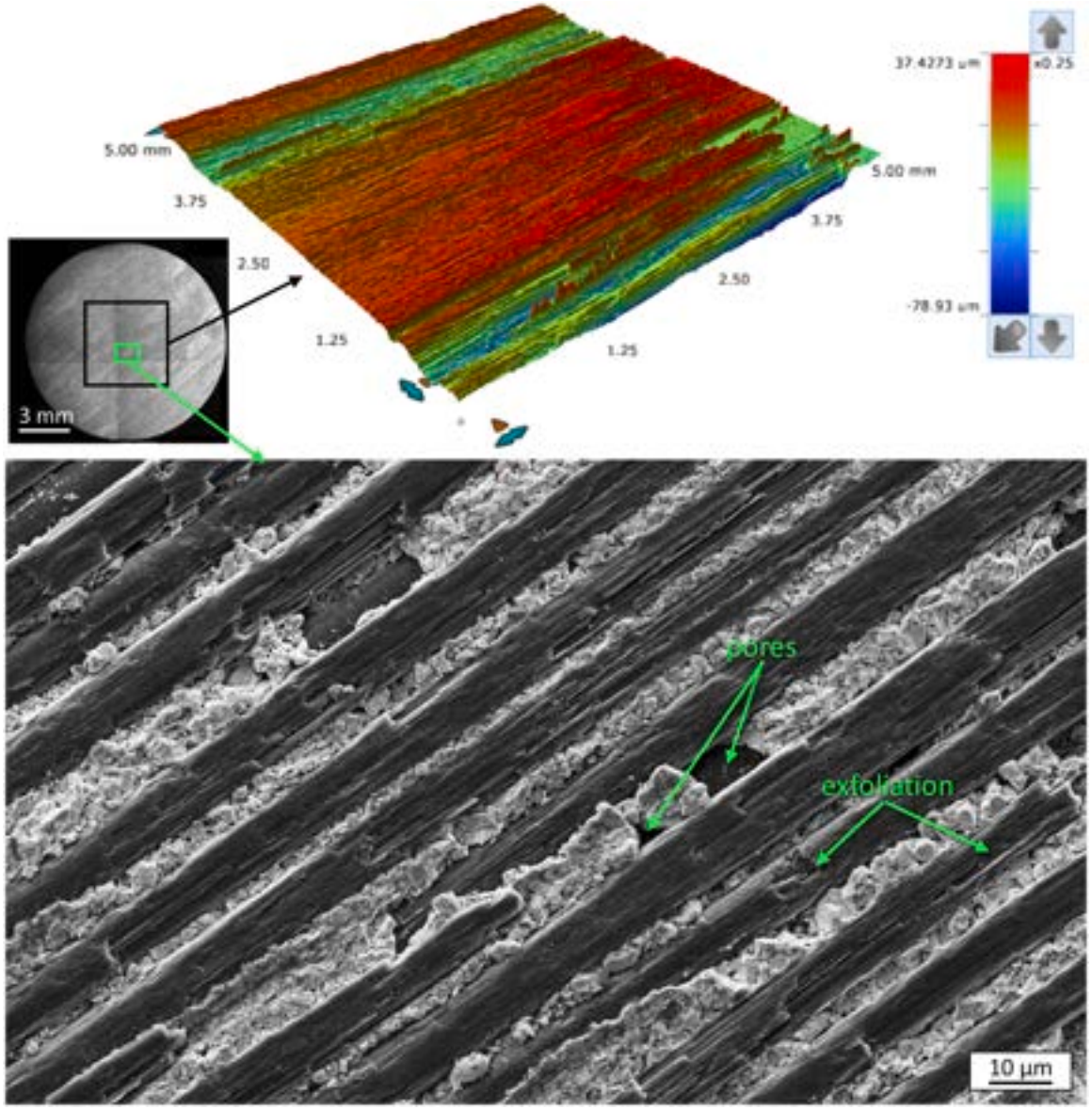

Fig. 3. SEM image of sample surface on the left, optical surface roughness measurement on the right: A 3D color-coded contour map of approximately twenty-five square millimeters of the black-boxed area in the sample surface center. At the bottom: detail of microstructure relative to the green-boxed area obtained by FE-SEM analysis.

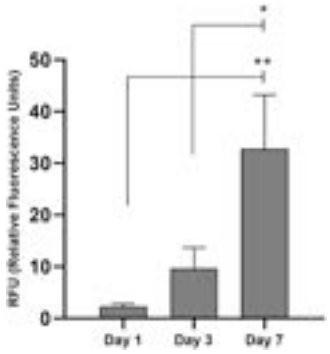

Fig. 4. Cell viability and proliferation evaluation by PrestoBlue Assay of fibroblasts seeded on the material at different time points. * p value $\leq$ 0.05; ** p value $\leq$ 0.01.

[15]), because the rigid ceramic matrix offered a greater level of support to the fibers, allowing to fully exploit both the matrix and fiber's potential, whereas the tensile strength was determined by features other than the fiber strength. An example of stress-strain curves of BAR and UBR samples tested under axial and radial directions is reported in Fig. 6. The behavior is similar to that observed on the samples tested under bending, displaying an elastic stress/strain behavior, followed by a small change in the slope which has been attributed to matrix cracking and fiber debonding in our previous works [10,21]. More studies are currently underway to fully explain this unusual behavior that is not found in other composites.

The compressive strength (σ_c) of UBR sample along the longitudinal direction was about 530 MPa and decreased by three times along the transverse direction, down to 170 MPa, due to the strongly anisotropic fiber configuration. For sample BAR, the two strength values along the different orientations were closer in value due to the more balanced configuration; σ_c along longitudinal direction was about 400 MPa and decreased by only 1.5 times along the transverse direction, 260 MPa. Even though samples UBR-T and BAR-T were tested in the same

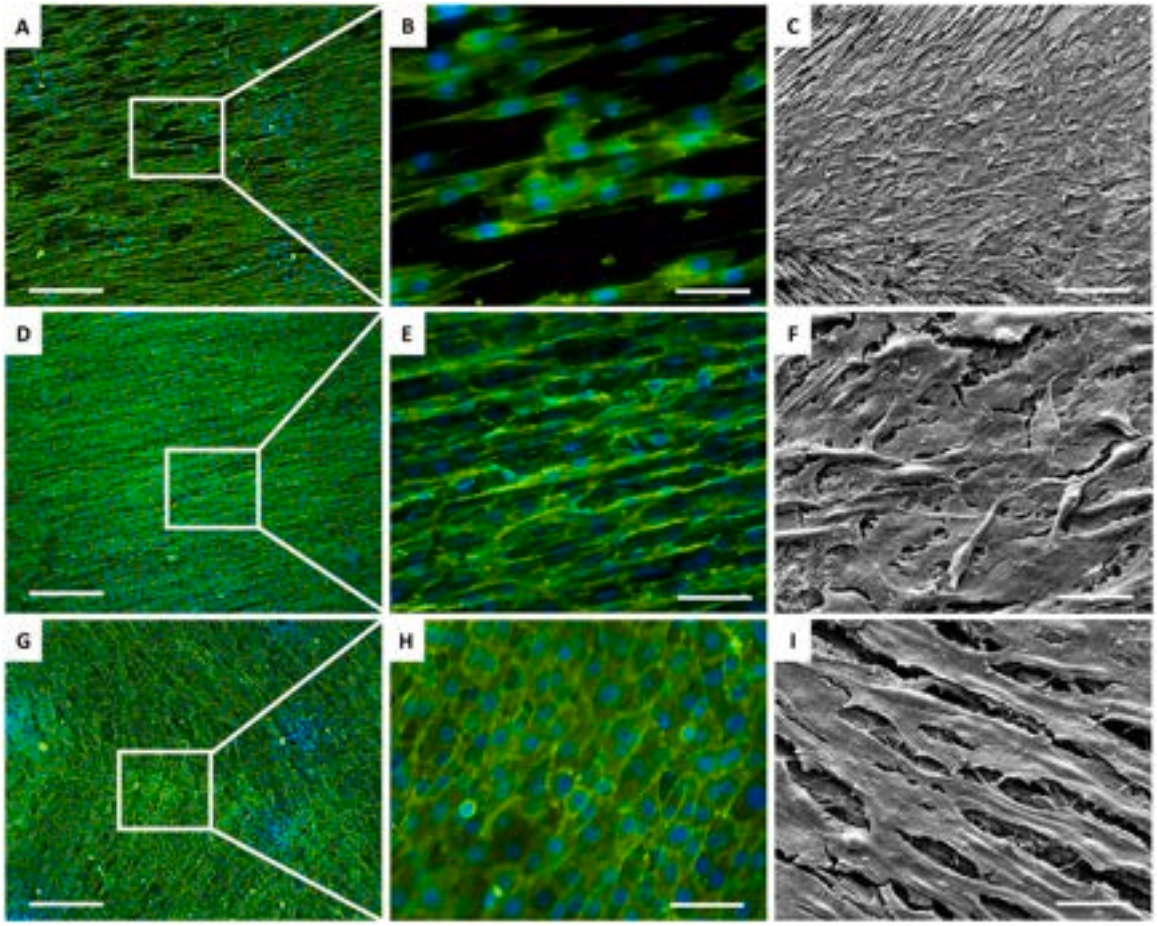

Fig. 5. Cell morphology evaluation. Fluorescence analysis of cell morphology after 1 (A, B), 3 (D, E) and 7 days (G-H). Cell nuclei in blue (DAPI) and F-actin filaments in green (Phalloidin) are reported. SEM analysis of cell morphology after 1 (C, F) and 3 days (I). Scale bar 200 μm (A, C, D and G) and 50 μm (B, E, F, H and I).

Table 1
Compression strength values at room temperature of sintered samples (L: longitudinal direction; T: transverse direction; UCS: ultimate compressive strength).

Sample	σ_c -T MPa	Strain at UCS %	σ_c -L MPa	Strain at UCS %
UBR	170 ± 20	3.5 ± 0.3	530 ± 50	1.2 ± 0.1
BAR	260 ± 20	2.7 ± 0.3	400 ± 20	2.1 ± 0.3

conditions, with the load applied perpendicularly to the fiber layer configuration, the two strength values were significantly different, with BAR-T showing a higher degree of resistance. This could be explained by the slightly different failure modes; due to the lack of reinforcement in the 90° orientation, sample UBR-T failed due to both compressive and shear stresses, whereas BAR-T failed mostly under compressive stresses.

Moreover, recently the tribological behavior of similar sintered UHTCMCs has been investigated. In particular, the performed tests were designed for braking applications, using UHTCMC-based pads against carbon fiber-reinforced carbon and SiC dual matrices composites (C/C-SiC) and steel disks, with dry contact at high pressures up to 3 MPa. The high values of coefficient of friction (COF) and the stable friction film formed on the abraded surface reducing wear rate make UHTCMCs very promising in application where they are subjected to frictional forces [22].

4. Discussion

Biocompatibility, adequate mechanical performance, absence of corrosion inside the human body and easy manufacturing are the main features that should be taken in account for designing promising novel prosthesis for hard tissue such as stem for hip prosthesis and dental screws that could replace the metal alloys-based implants currently used in clinical routine despite their limitations.

We were inspired in selecting UHTCMCs for this study by reading some recent works focused on ultra-high temperature ceramic (UHTC) coated titanium alloy. They discovered the ability of metal diboride coating, such as TaB_2 [23] and TiB_2 [24–26], in biological activities. In detail, the results of Zhang [23] on TaB_2 indicated that the inflammatory response caused by boron was moderate and more effective than only tantalum. In fact, TaB_2 coating revealed that macrophages on the Ta-B group were polarized into M2 macrophages compared with Ta group, and this polarization state is known to contribute to anti-inflammatory response promoting tissue remodeling and repair [27,28]. In addition, since boron is an essential trace element for bone health, TaB_2 coating has shown to enhance the osteogenic differentiation of mesenchymal stem cells [29,30]. Although no specific studies on the bioactivity of ZrB_2-based materials have been reported in the literature, we expected similar biocompatibility behavior to that of the other metal diborides (TiB_2 and TaB_2) as later verified in this study. Indeed, a few reports have suggested their similarity to TiB_2 and TaB_2 in terms of the partial hydrolysis of ZrB_2-based ceramics in various aqueous solutions (cell-free experiments) [31–36], resulting in the formation of soluble metal hydroxides and borates. In addition to their biocompatibility potential, C/ZrB_2-SiC material is much lighter compared to TaB_2-based materials and shows better machinability compared to TiB_2-based materials.

Previous attempts to strengthen silicon nitride ceramics [37], titanium alloys [38–41] or medical carbon/carbon [42,43] in existing

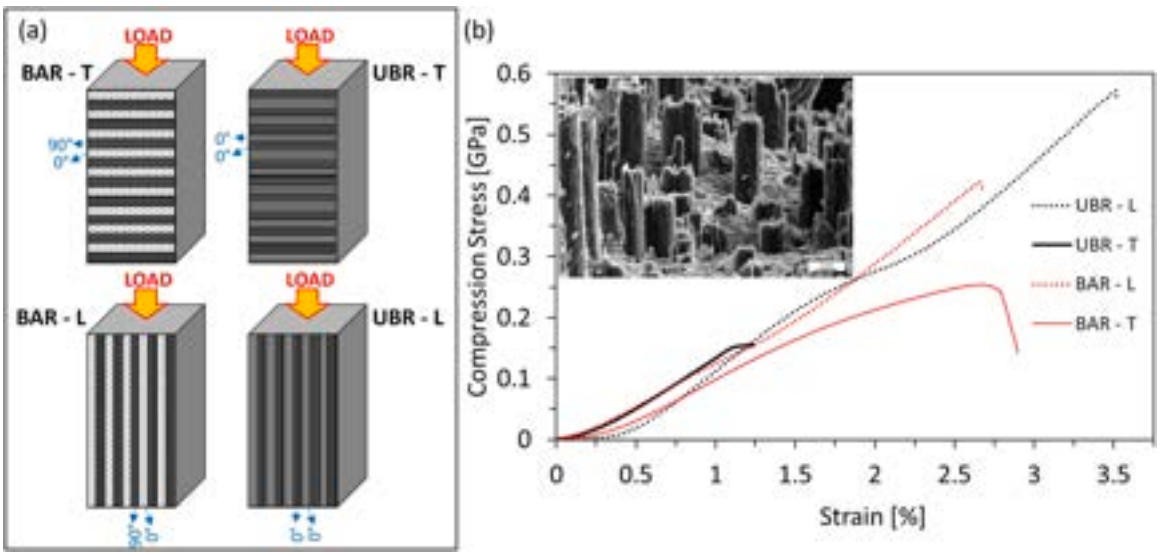

Fig. 6. (a) Sketch of specimens under longitudinal and transverse compression highlighting fiber layer orientation (0° and 90°); (b) stress-strain curves obtained through compression tests of UBR sample (black curves) and BAR sample (red curves) under transverse direction (solid line) and longitudinal direction (dashed line). Only one curve per sample is shown as an example. All values were consistent and with narrow dispersion. The inset in graph is a fracture surface micrograph of UBR-L specimen.

prostheses have had some limitations (e.g. titanium: tribocorrosion; carbon/carbon: low wear resistance; ceramics: fragile fracture).

Zirconia, also called "ceramic steel" [44], has been introduced in the biomedical field for replacing metallic materials due its high biocompatibility and mechanical properties [45], finding wide application in medicine for orthopedic implants and prostheses [46] and becoming a prevalent biomaterial in dentistry and dental implantology [47,48]. However, monolithic zirconia has some limitations for endosseous implants due to its ultralow chemical reactivity for osteogenic cell stimulation and high elastic modulus (>200 GPa), which is significantly higher than that recorded on cortical bone resulting in stress-shielding and peri-implant bone loss [49,50].

High brittleness of ceramics (including zirconia) makes them highly prone to surface damage during machining and the occurrence of microcracks under loading conditions, that could lead to material degradation and harmful medical conditions. UHTCMCs have been designed for significantly more demanding conditions and can offer solutions to these issues. For example, the extraction of ceramic or titanium prostheses can be a challenging procedure due to the eventuality of bone breakdown during revision. Nevertheless, sintered UHTCMs, if appropriately stressed by shear, may facilitate prosthesis/bone detachment at the carbon fiber/bone interface, which could potentially limit collateral damage during prosthesis revision procedures. It is worth noting that the lubricating properties of the carbon fibers are balanced by the ceramic matrix of the material, which helps to maintain stability and prevent excessive movement of the prosthesis.

Representative values of the properties of titanium alloys, as Ti–6Al–4 V ELI the most common biomaterial used for bone replacements and reconstructions [38,51], sintered silicon nitride [37], yttria stabilized zirconia (Y-TZP) which is preferred to other zirconia ceramics because of its unique balance of toughness and strength [52], carbon/carbon composite used for implants [42,43,53], and sintered UHTCMCs [10,54–56] are reported in Table 2.

Fiber-reinforced ZrB_2-SiC composites possess promising properties and may be emerging in the next future as novel bio-carboceramics for a multitude of medical applications in which superior strength, low

Table 2
Typical physical and mechanical properties at room temperature for titanium alloy Ti–6Al–4 V ELI, sintered Si_3N_4 and yttria stabilized zirconia (Y-TZP), carbon/carbon composites for medical devices, and sintered C_f/ZrB_2-SiC.

		Ti–6Al–4V ELI [38,51,57,58]	Si_3N_4 [37]	Y-TZP [52,59]	Carbon/carbon [42,43,53]	Sintered UHTCMCs This work, [10,54–56]
Type of failure		Ductile	Brittle	Brittle	Non-brittle	Non-brittle
Architecture of fibers		-	-	-	n.r.	0/90°
Density	g cm^{-3}	4.26–4.43	3.24–3.27	5.85–6.10	1.4–1.8	3.7 ± 0.3
Porosity	%	< 0.2	< 0.2	n.r.	8–12	7 ± 4
Young's modulus, E	GPa	105–122	295	200–210	5–12	138 ± 17 25 ± 3$^{\perp}$
Shear modulus, G	GPa	41–45	n.r.	n.r.	n.r.	27 ± 7
RT Flexural strength, σ_f	MPa	120–180	990	900–1200	45–130	220 ± 42 23 ± 9$^{\perp}$
Compressive strength, σ_c	MPa	1530–1590	3000	2000–2500	90–110	400 ± 20 260 ± 20$^{\perp}$
RT Tensile strength, σ_t	MPa	860–1160	Not applicable	Not applicable	80–170	120 ± 7
Toughness, K_{IC}	MPa $m^{1/2}$	91–100	6	7–10	n.r.	7 ± 1
Coefficient of thermal expansion, α	10^{-6} °C^{-1}	8.6–9.7	1.4–3.2	10.3–11.0	n.r.	4.2 ± 0.1 8.0 ± 0.4$^{\perp}$
Thermal conductivity, k_{th}	W m^{-1} K^{-1}	6.6–6.7	22	2.2–2.5	n.r.	140.0 28.1$^{\perp}$

n.r.: not reported; $^{\perp}$ Properties along the pile-up direction and measured on bars vertically machined.

deformability, damage tolerance, tribocorrosion/wear resistance and good machinability in complex shapes are required. In light of all these beneficial properties, a preliminary assessment of the cytotoxicity was evaluated for the first time. A complete absence of negative effects on cell adhesion, viability, proliferation and morphology was verified in vitro up to 7 days of culture. These preliminary biological results, together with the maturity of manufacturing readiness of UHTCMCs to realize components of complex geometry already achieved by our group [10,15], could extend the use of UHTCMCs beyond aerospace applications, for biomedical purposes such as the manufacturing of load-bearing hip- and knee endoprosthetic implants, screws, spinal intervertebral spacers and others (Fig. 7). Both the forming and machining technology employed for the fabrication of aerospace prototypes could be easily tuned to address the complexity and dimension requirements of hard tissue implants.

5. Conclusions

In this work, carbon fiber-reinforced ZrB_2-SiC composites were for the first time designed and fabricated for the use in the biomedical field.

The resulting homogeneous microstructure and fiber distribution was used as testing surface to verify the biological performance of these materials. The preliminary in vitro biological screening of cell behavior when in contact with these composites showed the absence of cytotoxicity.

The incorporation of a carbon fiber preform mitigated the intrinsic brittleness of ceramics, achieving improved damage tolerance and leading to a non-brittle failure, beyond a lower specific weight. The already known excellent mechanical properties (e.g. elastic modulus, flexural strength, tensile strength, and wear resistance) of these novel composites were completed by good compression resistance. Specifically, the compressive strength was over 500 MPa and 150 MPa, in longitudinal and transverse direction respectively, for composite with unbalanced carbon fiber architecture, while values of about 400 MPa in longitudinal direction and 260 MPa in transverse one were achieved with a balanced reinforcement. These results suggested that these composites exhibit a trade-off between mechanical performance and failure mode.

Therefore, the aerospace grade UHTCMCs appear to be a promising solution, although unconventional, for biological environment since they offer unique mechanical characteristics and biocompatibility, which are ideal for use as endoprosthesis for hard tissue. Although promising, the results should be supported by extensive in vitro investigations with different cell types to better clarify cell behavior in terms of cellular and molecular response, and particularly in vivo tests using animal models to assess the safety and effectiveness of a medical intervention before testing in humans.

CRediT authorship contribution statement

Luca Zoli: Conceptualization, Methodology, Writing – original draft, Data curation. **Francesca Servadei:** Investigation, Data curation, Writing – original draft. **Giada Bassi:** Investigation, Writing – originaldraft. **Arianna Rossi:** Investigation, Writing – original draft. **Monica Montesi:** Resources, Writing – review &editing. **Antonio Vinci:** Investigation, Writing – review & editing. **Diletta Sciti:** Funding acquisition, Writing –review & editing. **Silvia Panseri:** Conceptualization, Project administration, Writing – review & editing.

Funding

This work was supported by the European Union's Horizon 2020 "Research and innovation Programme" [grant agreement No 685594 (C3HARME)].

Fig. 7. Example of a screw and a nut machined by a sintered UHTCMC item produced by our group as concrete examples of components with complex geometry.

Declaration of Competing Interest

The authors declare that they have no known competing financial interests or personal relationships that could have appeared to influence the work reported in this paper.

Data Availability

The raw/processed data required to reproduce these findings cannot be shared at this time as the data also forms part of an ongoing study. Data will be made available on request.

Acknowledgments

The authors wish to thank C. Melandri for optical profilometer analysis.

References

[1] X. Du, S.S. Lee, G. Blugan, S.J. Ferguson, Silicon nitride as a biomedical material: an overview, Int. J. Mol. Sci. 23 (2022) 6551, https://doi.org/10.3390/ijms23126551.
[2] G. Pezzotti, Silicon nitride: a bioceramic with a gift, ACS Appl. Mater. Interfaces 11 (2019) 26619–26636, https://doi.org/10.1021/acsami.9b07997.
[3] S. Saddow, Silicon carbide technology for advanced human healthcare applications, Micromachines 13 (2022) 346, https://doi.org/10.3390/mi13030346.
[4] R. Bai, Q. Sun, Y. He, L. Peng, Y. Zhang, L. Zhang, W. Lu, J. Deng, Z. Zhuang, T. Yu, Y. Wei, Ceramic toughening strategies for biomedical applications, Front. Bioeng. Biotechnol. 10 (2022), https://doi.org/10.3389/fbioe.2022.840372.
[5] J. Wilson, Metallic biomaterials: state of the art and new challenges, in: Fundam. Biomater. Met., Woodhead Publishing, 2018, pp. 1–33, https://doi.org/10.1016/B978-0-08-102205-4.00001-5.
[6] B.G.X. Zhang, D.E. Myers, G.G. Wallace, M. Brandt, P.F.M. Choong, Bioactive coatings for orthopaedic implants-recent trends in development of implant coatings, Int. J. Mol. Sci. 15 (2014) 11878–11921, https://doi.org/10.3390/ijms150711878.
[7] J.M. Sadowska, K.J. Genoud, D.J. Kelly, F.J. O'Brien, Bone biomaterials for overcoming antimicrobial resistance: advances in non-antibiotic antimicrobial approaches for regeneration of infected osseous tissue, Mater. Today 46 (2021) 136–154, https://doi.org/10.1016/J.MATTOD.2020.12.018.
[8] M.M. Stevens, Biomaterials for bone tissue engineering, Mater. Today 11 (2008) 18–25, https://doi.org/10.1016/S1369-7021(08)70086-5.
[9] M. Mbogori, A. Vaish, R. Vaishya, A. Haleem, M. Javaid, Poly-Ether-Ether-Ketone (PEEK) in orthopaedic practice- a current concept review, J. Orthop. Rep. 1 (2022) 3–7, https://doi.org/10.1016/j.jorep.2022.03.013.
[10] D. Sciti, L. Zoli, T. Reimer, A. Vinci, P. Galizia, A systematic approach for horizontal and vertical scale up of sintered ultra-high temperature ceramic matrix composites for aerospace – advances and perspectives, Compos. Part B Eng. 234 (2022), 109709, https://doi.org/10.1016/j.compositesb.2022.109709.
[11] A. Vinci, T. Reimer, L. Zoli, D. Sciti, Influence of pressure on the oxidation resistance of carbon fiber reinforced ZrB_2/SiC composites at 2000 and 2200 °C, Corros. Sci. 184 (2021), https://doi.org/10.1016/j.corsci.2021.109377.
[12] F. Servadei, L. Zoli, A. Vinci, P. Galizia, D. Sciti, Significant improvement of the self-protection capability of ultra-high temperature ceramic matrix composites, Corros. Sci. 189 (2021), 109575, https://doi.org/10.1016/j.corsci.2021.109575.
[13] B. Mohammadzadeh, S. Jung, T.H. Lee, Q. Van Le, J.H. Cha, H.W. Jang, S.H. Lee, J. Kang, M. Shokouhimehr, Manufacturing ZrB_2-SiC-TaC composite: potential application for aircraft wing assessed by frequency analysis through finite element model, Materials 13 (2020), https://doi.org/10.3390/ma13102213.
[14] L. Zoli, A. Vinci, P. Galizia, C.F. Gutièrrez-Gonzalez, S. Rivera, D. Sciti, Is spark plasma sintering suitable for the densification of continuous carbon fibre -

UHTCMCs? J. Eur. Ceram. Soc. 40 (2020) 2597–2603, https://doi.org/10.1016/j.jeurceramsoc.2019.12.004.
[15] D. Sciti, P. Galizia, T. Reimer, A. Schoberth, C.F. Gutiérrez-Gonzalez, L. Silvestroni, A. Vinci, L. Zoli, Properties of large scale ultra-high temperature ceramic matrix composites made by filament winding and spark plasma sintering, Compos. Part B Eng. 216 (2021), https://doi.org/10.1016/j.compositesb.2021.108839.
[16] H. Faulstich, S. Zobeley, G. Rinnerthaler, J.V. Small, Fluorescent phallotoxins as probes for filamentous actin, J. Muscle Res. Cell Motil. 9 (1988) 370–383, https://doi.org/10.1007/BF01774064.
[17] L. Zoli, D. Sciti, A. Vinci, P. Galizia, F. Monteverde, S. Failla, L. Silvestroni, Ultra-high temperature ceramic matrix composites, Encycl. Mater. Tech. Ceram. Glas (2021) 340–352, https://doi.org/10.1016/b978-0-12-818542-1.00023-0.
[18] D. Bray, S. Ba, Ceramic engineering and science proceedings, Ceram. Eng. Sci. Proc. 29 (1988) 553–558.
[19] A. Vinci, L. Zoli, E. Landi, D. Sciti, Oxidation behaviour of a continuous carbon fibre reinforced ZrB_2–SiC composite, Corros. Sci. 123 (2017) 129–138, https://doi.org/10.1016/j.corsci.2017.04.012.
[20] F. Servadei, L. Zoli, P. Galizia, C. Melandri, D. Sciti, Preparation of UHTCMCs by hybrid processes coupling polymer infiltration and pyrolysis with hot pressing and vice versa, J. Eur. Ceram. Soc. 42 (2022) 2118–2126, https://doi.org/10.1016/j.jeurceramsoc.2021.12.039.
[21] P. Galizia, D. Sciti, Disclosing residual thermal stresses in UHT fibre-reinforced ceramic composites and their effect on mechanical behaviour and damage evolution, Compos. Part B Eng. 248 (2023), 110369, https://doi.org/10.1016/J.COMPOSITESB.2022.110369.
[22] M. Mor, M. Meiser, N. Langhof, A. Vinci, S. Failla, B. Alber-Laukant, S. Tremmel, S. Schafföner, D. Sciti, Tribological behavior of carbon fiber reinforced ZrB_2 based ultra high temperature ceramics, J. Eur. Ceram. Soc. (2023), https://doi.org/10.1016/J.JEURCERAMSOC.2023.05.019.
[23] R. Li, G. Liu, L. Yang, Y. Qing, X. Tang, D. Guo, K. Zhang, Y. Qin, Tantalum boride as a biocompatible coating to improve osteogenesis of the bionano interface, J. Biomed. Mater. Res. Part A. 108 (2020) 1726–1735, https://doi.org/10.1002/JBM.A.36940.
[24] M. Niinomi, M. Nakai, S. Yonezawa, X. Song, L. Wang, Effect of TiB_2 or Y_2O_3 additions on mechanical biofunctionality of Ti-29Nb-13Ta-4.6Zr for biomedical applications, Ceram. Trans. 228 (2011) 75–81, https://doi.org/10.1002/9781118144565.CH8.
[25] A. Ebrahimi, H. Esfahani, O. Imantalab, A. Fattah-Alhosseni, Biological, antibacterial activities and electrochemical behavior of borided commercially pure titanium in BSA-containing PBS, Trans. Nonferrous Met. Soc. China 30 (2020) 944–957, https://doi.org/10.1016/S1003-6326(20)65267-0.
[26] N. Singh, R. Ummethala, K.B. Surreddi, J. Jayaraj, R. Sokkalingam, M. Rajput, K. Chatterjee, K.G. Prashanth, Effect of TiB_2 addition on the mechanical and biological response of spark plasma sintered Ti6Al7Nb matrix composites, J. Alloy. Compd. 924 (2022), 166502, https://doi.org/10.1016/j.jallcom.2022.166502.
[27] Q.L. Ma, L.Z. Zhao, R.R. Liu, B.Q. Jin, W. Song, Y. Wang, Y.S. Zhang, L.H. Chen, Y. M. Zhang, Improved implant osseointegration of a nanostructured titanium surface via mediation of macrophage polarization, Biomaterials 35 (2014) 9853–9867, https://doi.org/10.1016/J.BIOMATERIALS.2014.08.025.
[28] A. Mantovani, S.K. Biswas, M.R. Galdiero, A. Sica, M. Locati, Macrophage plasticity and polarization in tissue repair and remodelling, J. Pathol. 229 (2013) 176–185, https://doi.org/10.1002/PATH.4133.
[29] P.N. Taşlı, A. Doğan, S. Demirci, F. Şahin, Boron enhances odontogenic and osteogenic differentiation of human tooth germ stem cells (hTGSCs) in vitro, Biol. Trace Elem. Res. 153 (2013) 419–427, https://doi.org/10.1007/s12011-013-9657-0.
[30] X. Ying, S. Cheng, W. Wang, Z. Lin, Q. Chen, W. Zhang, D. Kou, Y. Shen, X. Cheng, F.A. Rompis, L. Peng, C.Z. Lu, Effect of boron on osteogenic differentiation of human bone marrow stromal cells, Biol. Trace Elem. Res. 144 (2011) 306–315, https://doi.org/10.1007/s12011-011-9094-x.
[31] C. Monticelli, A. Bellosi, M. Dal Colle, Electrochemical behavior of ZrB_2 in aqueous solutions, J. Electrochem. Soc. 151 (2004) B331, https://doi.org/10.1149/1.1739219/XML.
[32] Z. Wang, Q. Zhao, L. Jing, Z. Wu, X. Sun, Corrosion behavior of ZrB_2–SiC–Graphite ceramic in strong alkali and strong acid solutions, Ceram. Int. 42 (2016) 2926–2932, https://doi.org/10.1016/J.CERAMINT.2015.10.075.
[33] H. Yang, J. Zhang, J. Li, F. Chen, Q. Shen, L. Zhang, Electrochemical corrosion behavior of zirconium diboride ceramic in concentrated alkaline solutions, Mater. Res. Express 5 (2018), https://doi.org/10.1088/2053-1591/aae019.
[34] J. Yin, H. Zhang, Y. Yan, Z. Huang, X. Liu, Y. Yang, D. Jiang, Hydrolysis behavior of zirconium diboride during attrition milling, Mater. Chem. Phys. 133 (2012) 8–15, https://doi.org/10.1016/j.matchemphys.2011.11.004.
[35] D.L. Feke, Stability and rheology of dispersions of silicon nitride and silicon carbide, 1987. https://ntrs.nasa.gov/citations/19870016043 (Accessed 22 February 2023).
[36] K. Lindqvist, E. Carlström, M. Persson, R. Carlsson, Organic silanes and titanates as processing additives for injection molding of ceramics, J. Am. Ceram. Soc. 72 (1989) 99–103, https://doi.org/10.1111/J.1151-2916.1989.TB05960.X.
[37] QSIL Ingenieurkeramik GmbH, Material Data Sheet for Hot Pressed Silicon Nitride (black), 2020. https://www.qsil-ceramics.com/fileadmin/user_upload/downloads/Datenblätter/SN-HP_black_ENG_.pdf (Accessed 27 February 2023).
[38] H.J. Rack, J.I. Qazi, Titanium alloys for biomedical applications, Mater. Sci. Eng. C. 26 (2006) 1269–1277, https://doi.org/10.1016/J.MSEC.2005.08.032.
[39] D.F. Williams, in: D.F. Williams (Ed.), Titanium and Titanium Alloys, Biocompat. Clin. Implant Mater., CRC Press, Boca Raton, FL, USA, 1982, pp. 10–44.
[40] R.M. Pillar, G.C. Weatherly, Development in implant alloys, in: D.F. Williams (Ed.), Clin. Rev. Biocompat, 1, CRC Press, Boca Raton, FL, USA, 1982, pp. 371–473.
[41] D.F. Williams, Biological effects of titanium, in: D.F. Williams (Ed.), Syst. Asp. Biocompat., CRC Press, Boca Raton, FL, USA, 1982, pp. 170–177.
[42] X. Gao, S. Wang, Y. Xu, H. Li, H. Zhao, X. Pan, Ferulic acid and PDMS modified medical carbon materials for artificial joint prosthesis, PLoS One 13 (2018), e0203542, https://doi.org/10.1371/JOURNAL.PONE.0203542.
[43] I.V. Gurin, Medical Products and Medical Device Engineering CARBON-CARBON IMPLANTS, (n.d.). https://files.nas.gov.ua/NASDevelopmentsBook/PDF/0728e.pdf (Accessed 27 February 2023).
[44] R.C. Garvie, R.H. Hannink, R.T. Pascoe, Ceramic steel?, Nat. 1975 2585537. 258, 1975, pp. 703–704. https://doi.org/10.1038/258703a0.
[45] L. Vaiani, A. Boccaccio, A.E. Uva, G. Palumbo, A. Piccininni, P. Guglielmi, S. Cantore, L. Santacroce, I.A. Charitos, A. Ballini, Ceramic materials for biomedical applications: an overview on properties and fabrication processes, J. Funct. Biomater. 14 (146) (2023) 146, https://doi.org/10.3390/JFB14030146.
[46] C. Piconi, G. Maccauro, F. Muratori, E. Brach Del Prever, Alumina and zirconia ceramics in joint replacements, J. Appl. Biomater. Biomech. 1 (2003) 19–32.
[47] A. Della Bona, O.E. Pecho, R. Alessandretti, Zirconia as a dental biomaterial, Mater 2015 8 (8) (2015) 4978–4991, https://doi.org/10.3390/MA8084978.
[48] J. Grech, E. Antunes, Zirconia in dental prosthetics: a literature review, J. Mater. Res. Technol. 8 (2019) 4956–4964, https://doi.org/10.1016/J.JMRT.2019.06.043.
[49] C.I. Resende-Gonçalves, N. Sampaio, J. Moreira, O. Carvalho, J. Caramês, M. C. Manzanares-Céspedes, F. Silva, B. Henriques, J. Souza, Porous zirconia blocks for bone repair: an integrative review on biological and mechanical outcomes, Ceramics 5 (2022) 161–172, https://doi.org/10.3390/CERAMICS5010014/S1.
[50] T.J. Marrow, S.G. Roberts, A.K. Pearce-Higgins, The brittle/ductile transition in cubic stabilised zirconia, J. Eur. Ceram. Soc. 14 (1994) 447–453, https://doi.org/10.1016/0955-2219(94)90083-3.
[51] S. Suresh, C.N. Sun, S. Tekumalla, V. Rosa, S.M. Ling Nai, R.C.W. Wong, Mechanical properties and in vitro cytocompatibility of dense and porous Ti–6Al–4V ELI manufactured by selective laser melting technology for biomedical applications, J. Mech. Behav. Biomed. Mater. 123 (2021), 104712, https://doi.org/10.1016/j.jmbbm.2021.104712.
[52] C. Piconi, G. Maccauro, Zirconia as a ceramic biomaterial, Biomaterials 20 (1999) 1–25, https://doi.org/10.1016/S0142-9612(98)00010-6.
[53] Z. Tan, X. Zhang, J. Ruan, J. Liao, F. Yu, L. Xia, B. Wang, C. Liang, Synthesis, structure, and properties of carbon/carbon composites artificial rib for chest wall reconstruction, Sci. Rep. 11 (2021) 1–12, https://doi.org/10.1038/s41598-021-90951-8.
[54] L. Zoli, D. Sciti, Efficacy of a ZrB_2–SiC matrix in protecting C fibres from oxidation in novel UHTCMC materials, Mater. Des. 113 (2017) 207–213, https://doi.org/10.1016/j.matdes.2016.09.104.
[55] A. Vinci, L. Zoli, D. Sciti, C. Melandri, S. Guicciardi, Understanding the mechanical properties of novel UHTCMCs through random forest and regression tree analysis, Mater. Des. 145 (2018) 97–107, https://doi.org/10.1016/j.matdes.2018.02.061.
[56] J. Binner, M. Porter, B. Baker, J. Zou, V. Venkatachalam, V.R. Diaz, A. D'Angio, P. Ramanujam, T. Zhang, T.S.R.C. Murthy, Selection, processing, properties and applications of ultra-high temperature ceramic matrix composites, UHTCMCs–a review, Int. Mater. Rev. 65 (2020) 389–444, https://doi.org/10.1080/09506608.2019.1652006.
[57] Titanium Ti-6Al-4V ELI Datasheet, (n.d.). https://www.upmet.com/sites/default/files/datasheets/ti-6al-4v-eli.pdf (Accessed 7 June 2023).
[58] Titanium Ti-6Al-4V ELI (Grade 23), Annealed, (n.d.). https://www.matweb.com/search/datasheet_print.aspx?matguid=c4297fb8f1094da189732c224e3be1ed (Accessed 7 June 2023).
[59] Yttria Stabilized Zirconia, YSZ, (n.d.). https://www.matweb.com/search/datasheet_print.aspx?matguid=4e3988dd9adb4d1ca37a1b2cbab87d9a (Accessed 7 June 2023).